MELT FORMATION ON SHATTER CONE SURFACES IN SANDSTONE, PART II: MELT COMPOSITION. C. Hamann[1], J. Wilk[2], L. Hecht[1], and T. Kenkmann[2]. [1]Museum für Naturkunde, Leibniz-Institut für Evolutions- und Biodiversitätsforschung, Invalidenstraße 43, 10115 Berlin, Germany. [2]Institut für Geo- und Umweltnaturwissenschaften, Albert-Ludwigs-Universität Freiburg, Albertstraße 23b, 79104 Freiburg im Breisgau, Germany (christopher.hamann@mfn–berlin.de, jakob.wilk@geologie.uni–freiburg.de).

Introduction: Shatter cones are conical, striated rock fractures that occur either individually or as hierarchically related sets. They are the characteristic form of rock fractures in impact structures and are currently believed to be the only unequivocal macroscopic fingerprint of impact events on Earth (*e.g.*, [1]). However, their exact formation mechanism(s) remain enigmatic, and to date, several models of shatter cone formation exist. Most of them, in essence, link their formation to the presence of material heterogeneities in the trailing end of the shock wave (*e.g.*, [2, 3]), whereas other authors suggested that shatter cones form upon decompression [4]. Moreover, several reports of melt films on shatter cone surfaces (*e.g.*, [5, 6]) further impede our understanding of shatter cone formation, yet may allow to constrain pressure–temperature–time conditions during or immediately after shatter cone formation.

Here, we investigate silicate melt films on shatter cones from impact experiments performed in the context of the Multidisciplinary Experimental and Modeling Impact Research Network (MEMIN) [7].

Materials and Methods: A series of impact experiments was performed using the two-stage light-gas guns of the Fraunhofer Institut für Kurzzeitdynamik, Freiburg, Germany. Here, we report on experiments A15-5185 (5-mm-diameter aluminum projectile shot onto dry sandstone at 6.97 km/s) and E3-3384 (12-mm-diameter Campo del Cielo iron meteorite projectile shot onto water-saturated sandstone at 4.59 km/s). Shatter cone fragments were sampled and analyzed with white light interferometry [7]. Those fragments that show characteristic features of shatter cones were further investigated with analytical scanning electron microscopy, using 15 kV acceleration voltage and varying beam currents. Here, and in the companion abstract "*Melt Formation on Shatter Cone Surfaces in Sandstone, Part I: Surface Morphology*" by Wilk et al. (this volume), we present a detailed description of fresh melt features detected on experimentally produced shatter cones.

Results: The fragments we consider as shatter cones show slightly curved and conical geometries that are marked by fine striation patterns typical for shatter cones (*cf.* [7] and companion abstract). Usually, the striated surfaces are covered with thin films of melt-textured, glassy materials distinctly different from the sandstone underneath (Fig. 1; *cf.* companion abstract).

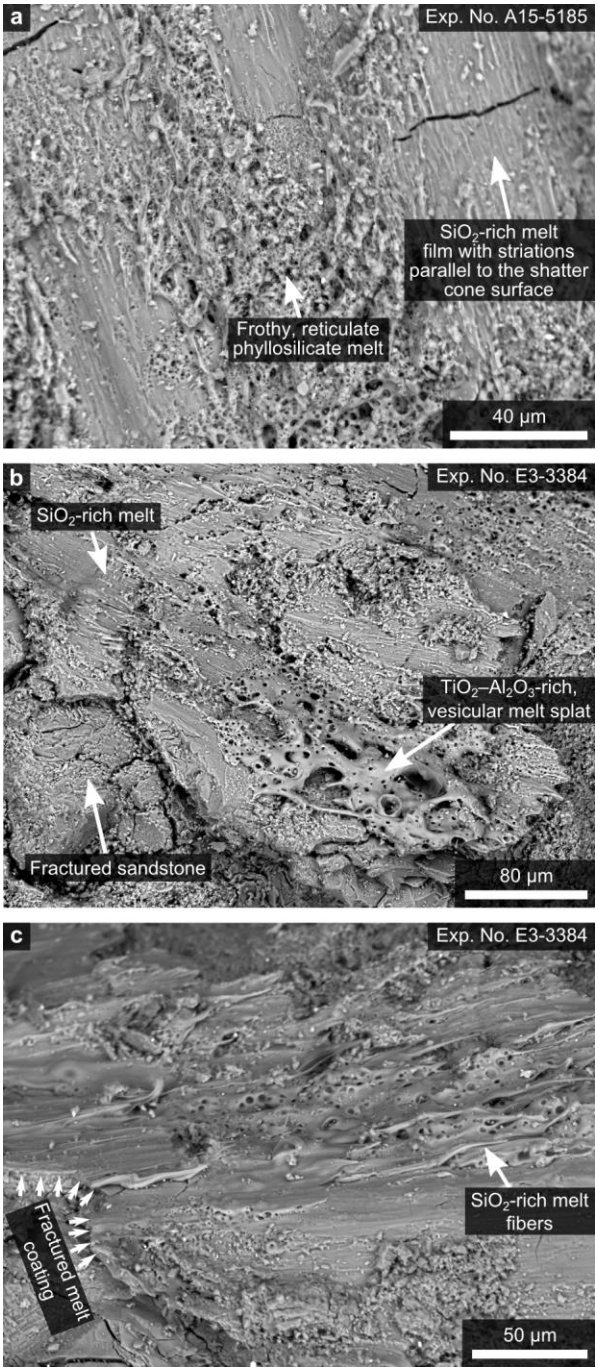

Fig. 1 BSE images of the melt films on top of the surfaces of three shatter cones from experiments with dry (Exp. No. A15-5185) and water-saturated (Exp. No. E3-3384) sandstone.

Melt textures: Three kinds of melts can usually be distinguished (Figs. 1 and 2): (i) a vesicle-poor, SiO_2-rich melt that either occurs as a smooth, striated film or as elongated, identically oriented, parallel, ropy fibers covering the striation surfaces, (ii) a vesicle-rich melt with high TiO_2 and Al_2O_3 contents that occurs randomly intercalated with the SiO_2-rich melt and, occasionally, also in the form of patchy splats and smears, and (iii) a frothy, reticulate melt that shows roughly the composition of accessory phyllosilicates. Often, these melts merge texturally (Fig. 1a, b), and elemental distribution maps (Fig. 2) indicate mixing of these melts.

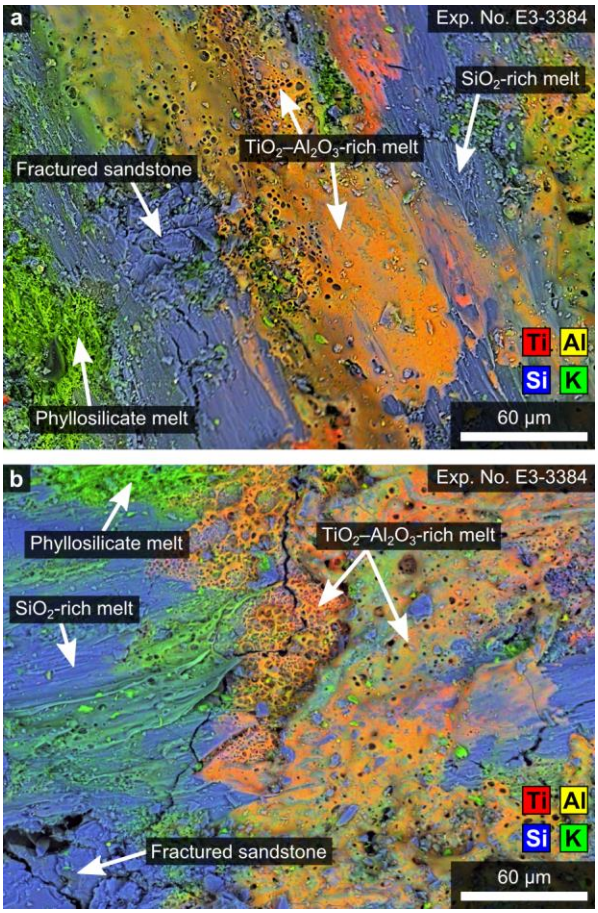

Fig. 2 Elemental distribution maps superimposed onto BSE images, illustrating differences in melt composition and mixing between quartz, phyllosilicates, and rutile melts.

Melt compositions: The melts described above differ markedly in composition (Figs. 2 and 3). The SiO_2-rich melt is not a pure quartz melt, as indicated by the presence of, on average, ~2 wt.% Al_2O_3 and TiO_2 (Fig. 3). Compared to the bulk sandstone, it is enriched in Ti, which is likely caused by additional melting of, and mixing with, accessory rutile. As emanating from Fig. 3, the vesicle-rich, TiO_2–Al_2O_3-rich melt is primarily a mixture of phyllosilicates and accessory rutile, which must have incorporated limited amounts of the SiO_2-rich melt and/or a pure quartz melt (lechatelierite). The frothy, reticulate melt closely mimics the composition of phyllosilicate minerals present in the target (Fig. 3). However, compared to the phyllosilicates, this melt is also enriched in Ti, closely following a mixing trend with rutile. Hence, limited mixing with a pure rutile and/or the TiO_2–Al_2O_3-rich melt is indicated.

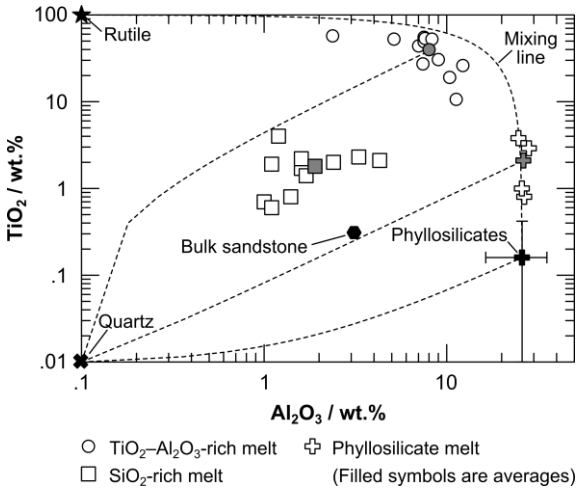

Fig. 3 Compositions of the sandstone components prior to impact and the shatter cone melt coatings, plotted in terms of TiO_2 and Al_2O_3 contents (Exp. No. E3-3384).

Discussion and Conclusions: Melting and mixing of quartz, phyllosilicates, and rutile requires temperatures in excess of 1842 °C (melting point of rutile at ambient pressure), as well as the simultaneous presence of coexisting monomineralic precursor melts that mix during the short time interval prior to solidification. This, together with the surface morphology of the melt textures (*cf.* companion abstract), indicates that the melt films most likely formed by a combination of shock and frictional heating, locally inducing high pressures (a few GPa?) and post-shock temperatures (>1842 °C) along the shatter cone surface. Moreover, the melt fibers document directional shear movement parallel to the shatter cone surface, whereas the vesicular melt splats may have accumulated and degassed at locations of pressure release. Our next steps are to more accurately constrain the *P–T* conditions that led to melting and lubrication of the striation surfaces.

Acknowledgments: MEMIN is funded by the DFG (FOR 887); these are projects Ke-732/22-1 and He-2893/8-2.

References: [1] Dietz R. S. (1960) *Science, 131,* 1781–1784. [2] Baratoux D. and Melosh H. J. (2003) *EPSL, 216,* 43–54. [3] Sagy A. et al. (2004) *JGR, 111,* 1–20. [4] Wieland F. et al. (2006) *M&PS, 41,* 1737–1759. [5] Gibson H. M. and Spray J. G. (1998) *M&PS, 33,* 329–336. [6] Pittarello L. et al. (2015) *M&PS, 50,* 1228–1243. [7] Wilk J. and Kenkmann T. (2015) *Bridging the Gap III,* Abstract #1066.